Construction and Building Materials 423 (2024) 135651

Contents lists available at ScienceDirect

Construction and Building Materials

journal homepage: www.elsevier.com/locate/conbuildmat

Review

Bond strength, failure criteria and calculation methods for adhesively bonded timber–concrete composites

Jens Frohnmüller *, Werner Seim

University of Kassel, Kurt-Wolters Straße 3, 34125 Kassel, Germany

ARTICLE INFO

Keywords:
Timber–concrete composites
Adhesives
Bond strength
Failure criteria
Cohesive zone model
Fracture mechanics
Hybrid timber construction

ABSTRACT

The bond strength of adhesively bonded timber–concrete composites (ATCC) with prefabricated concrete elements is usually described using the shear strength of the timber. This approach, however, often fails to consider the actual failure modes of the bondline and also the interaction between shear stresses and stresses perpendicular to the bondline has not yet been comprehensively understood. To address this limitation, a reliable calculation method is required, where stress determination, failure criterion, and stress analysis are clearly defined to accurately predict the bond failure of ATCC specimens. In this study, three linear-elastic calculation methods and one non-linear calculation method are presented along with corresponding failure criteria and strength parameters. Regarding validation, the predicted failure load is compared to experimental results from 186 ATCC bond specimens to assess the method's suitability. Based on the findings, appropriate calculation methods for a reliable prediction of the bond strength are recommended.

1. Introduction

A growing interest of research and industry in the technology of bonding timber to concrete has been observed in recent years. One major reason for this is that a more or less rigid bond is achieved, allowing the optimum utilization of the individual materials. Moreover, the use of adhesives for the interconnection allows one to work with prefabricated concrete elements ("prefabs"), eliminating the disadvantages of in situ concrete. In this way, the classic advantages of timber construction, such as a high degree of prefabrication, short construction times and low moisture input into the building, are retained, while, at the same time, a separate prefabrication of the individual components is possible.

This study focuses on adhesively bonded timber–concrete composites (ATCC) which are assembled with concrete prefabs. Adhesive bonding can be carried out either in a factory building or on the construction site, depending on the logistics boundary conditions. To meet the challenges of on-site processing, a comprehensive quality assurance concept was developed by Frohnmüller et al. [1]. This concept includes quality control of the components, conditions for execution and testing of reference samples.

The research on this topic has today reached a stage that allows the implementation of initial pilot projects [2,3], since questions of suitable materials and adhesives have been answered [4–8] and the long-term deformation behavior has also been investigated [9,10]. The bond strength of ATCC structures has usually been described with the shear strength of the timber [4,11]. If, however, other materials are being used for the construction of ATCC, such as beech with a large shear strength [12–14] or concrete parts with a comparatively low surface-tensile strength [15–18], then the failure can also occur in the concrete substrate or as a mixed failure in both the concrete and the timber. In this case, the resistance of the adhesive bondline is not clear, because neither the EC5 [19] nor the draft of the technical specification TS 19103 [20] provide sufficient information for the bond strength of concrete surfaces.

The failure modes, which could theoretically take place in the adhesive bondline, are depicted in Fig. 1. A stress verification must be performed in the engineering design process for the substrate failure modes FM1 and FM5. Adhesion failure FM2 or FM4 can usually be excluded by selecting a suitable adhesive and conducting a quality control system on the construction site [2,8,21]. Regarding adhesives and polymer mortars that meet the requirements for application, stiffness and adhesion, cohesion failure FM3 can generally be excluded in the verification process due to their high tensile and shear strength properties compared to timber or concrete.

It is usually required for structural adhesives, which are being used for timber constructions, that substrate failure occurs in all cases but never an adhesion or cohesion failure of the adhesive even for long-term testing of the durability. The bond failure can, therefore, be attributed exclusively to the strength of the timber and the concrete and takes place as a brittle failure, see Fig. 2.

* Corresponding author.
E-mail addresses: frohnmueller@uni-kassel.de (J. Frohnmüller), wseim@uni-kassel.de (W. Seim).

https://doi.org/10.1016/j.conbuildmat.2024.135651
Received 22 December 2023; Received in revised form 22 February 2024; Accepted 27 February 2024
Available online 22 March 2024

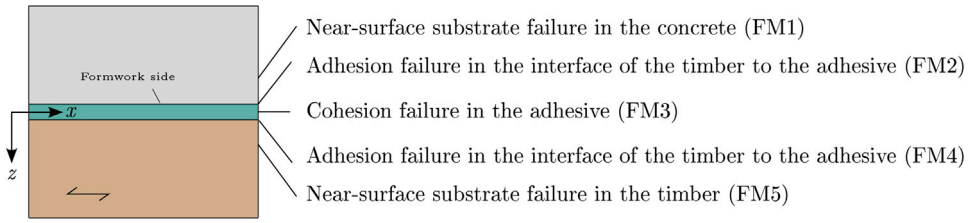

Fig. 1. ATCC bond failure — theoretical failure modes in the bondline.

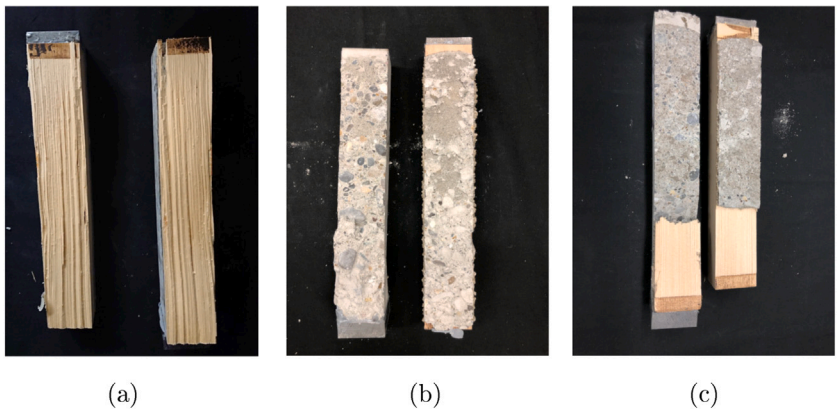

Fig. 2. Failure modes of bond specimens (a) Near-surface shear failure in timber — plan view (b) Near-surface shear failure in concrete — plan view (c) Mixed near-surface shear failure in timber and concrete — plan view.

Regarding the stress-verification design of the failure modes FM1 and FM5, open questions remain regarding the interaction of shear stresses and stresses perpendicular to the bondline because currently no generally applicable failure criterion is available for the adhesive joint. Size-effects are also repeatedly discussed [15,18]. The objective of this work, therefore, is to provide a reliable calculation method (model for stress determination + failure criterion + stress analysis) for the prediction of the bond failure of the adhesive bond of timber to concrete.

2. Materials and methods

2.1. Approach

First, models for stress determination and suitable failure criteria to describe the resistance of the ATCC bondline are determined based on approaches from the literature. A brief overview of the bond tests is then provided from which the experimental failure load $F_{u,exp,b}$ is derived. Subsequently, four calculation methods (AN, FE-S, FE-P, and FE-K) are introduced to predict the failure load $F_{u,cal,b}$, taking into account the strength parameters of timber and concrete. The shear strength parameter of the timber is hereby already determined considering the calculation methods. Then, $F_{u,cal,b}$ is calculated for each method for each test series. Regarding validation, a comparison is made between $F_{u,exp,b}$ and $F_{u,cal,b}$, which allows one to draw conclusions concerning the suitability of the model for stress calculation, the selected failure criteria, and material parameters considered in the failure criteria.

2.2. Models for the stress calculation

The models for stress determination, which have been chosen by the authors from the literature to analyse ATCC bond specimens can be categorized in analytical approaches [4–7,11,12,14,15,22], numerical approaches with a combined analysis of the stress peaks and stress interaction of shear and normal stresses perpendicular to the bondline [4, 22] and linear-elastic fracture mechanic (LEFM) approaches [4,6,11]. The models used in this study are introduced based on this assessment in Section 4.

2.3. Stress-based failure criteria

A comparatively simple failure criterion can be found under the assumption that failure is solely triggered by shear stresses. Failure occurs when the shear stress τ reaches the shear strength f_v.

$$\frac{\tau}{f_v} = 1 \tag{1}$$

No pure stress state occurs in most applications, but the actual stress state, instead, corresponds to a combination of different stress components, such as shear and normal stresses. There, it is often necessary to use failure criteria with which combined stress states can be predicted on the basis of uni-axial strength parameters, such as f_t, f_c or f_v. Since two different materials are combined in ATCC constructions, it is useful to choose a common definition of the coordinates. For a concrete surface, which is always defined as the formwork side, and a timber grain, which is always defined as parallel to the adhesive joint, the x-axis can be chosen parallel to the adhesive bondline along the length of the specimen, while the z-axis is oriented perpendicular to the adhesive bondline (see Fig. 1).

A failure criterion for timber has been proposed by Blaß& Krüger [23] based on tests from Spengler [24] and was experimentally validated for the ranges σ_z = 2.0 to −4.5 N/mm^2. Further failure criteria have been discussed by Akter & Bader [25], whereby the failure criterion given in the Swiss standard SIA 265 [26] involving the three parameters tension and compression strength perpendicular to the grain $f_{t,90}$ and $f_{c,90}$ and the shear strength f_v has led to superior results, see Eq. (2). This failure criterion is, thus, chosen for this study.

$$\left(\frac{f_{c,90}+\sigma_z}{f_{c,90}+f_{t,90}}\right)^2 + \left(\frac{\tau}{f_v}\right)^2 \cdot \left[1-\left(\frac{f_{c,90}}{f_{c,90}+f_{t,90}}\right)^2\right] = 1 \tag{2}$$

The application limits of Eq. (2) are set to $f_{t,90}$ and $f_{c,90}$, which is reasonable for analytical calculation methods where the compression

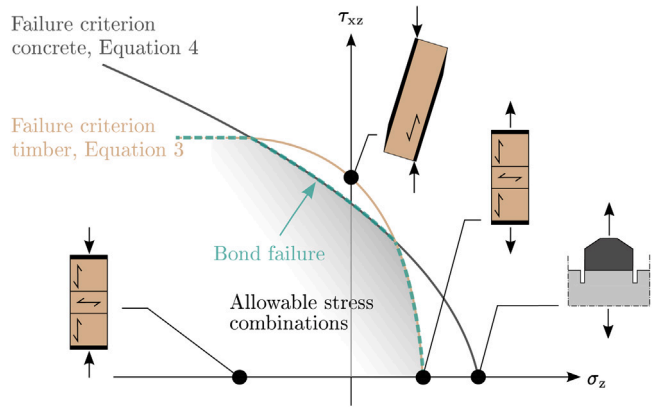

Fig. 3. Exemplary resistance of the adhesive bondline, depicted in the shear-normal stress diagram. Test set-ups of the timber taken from EN 408 [28], test set-up of the concrete taken from DIN 1542 [29] and DIN 1048 [30].

stresses perpendicular to the grain are assumed to be a constant stress block. These application limits in FE models with linear-elastic material parameters, however, could lead to inaccurate results, since stress peaks could exceed the compression strength in single FE elements. It is assumed that exceeding $f_{c,90}$ by individual bond stress pairs may be permissible due to local stress redistribution in the timber, since no compression failure perpendicular to the grain was observed in any of the bond tests analysed in this study. This assumption is also supported by literature sources, where stress combinations in the range up to about 1.4 times the compressive strength perpendicular to the grain have been allowed even for an analytical calculation of the stresses [23], which leads to:

$$\left.\begin{array}{l} \left(\frac{f_{c,90}+\sigma_z}{f_{c,90}+f_{t,90}}\right)^2 + \left(\frac{\tau}{f_v}\right)^2 \cdot \left[1-\left(\frac{f_{c,90}}{f_{c,90}+f_{t,90}}\right)^2\right] \quad \text{for } \sigma_z \le f_{c,90} \\ \left(\frac{\tau}{f_v}\right)^2 \cdot \left[1-\left(\frac{f_{c,90}}{f_{c,90}+f_{t,90}}\right)^2\right] \quad \text{for } \sigma_z > f_{c,90} \end{array}\right\} = 1 \tag{3}$$

Regarding the concrete surface, an example of a failure criterion is the so-called Mohr's envelope. The idea of Mohr's envelope was adapted by Austin et al. [27] and the surface tensile strength $f_{ct,surf}$ is used as the strength parameter, see Eq. (4). For $\sigma_z = 0$, the shear stresses corresponds to twice the value of $f_{ct,surf}$.

$$\frac{\tau}{\sqrt{4 \cdot f_{ct,surf} \cdot (f_{ct,surf} - \sigma_z)}} = 1 \tag{4}$$

Exemplarily, the resistance of the adhesive bondline is shown in the shear-normal stress diagram in Fig. 3 for an utilization of Eqs. (3) and (4). It can be seen that the decisive composite part for the material combination depicted changes.

2.4. Failure criteria based on fracture mechanics concepts

While stress-based failure criteria assume that bond failure occurs when the critical stress or the critical combination of stresses is reached, fracture mechanics concepts assume that bond failure occurs when the crack growing becomes unstable. LEFM concepts are suitable for the modeling of brittle failure modes such as tensile and shear failure of timber or concrete, where the fracture zone is small compared to the surrounding material [31].

For plane stress situations, the failure modes can be separated in Mode I (tension perpendicular to the bondline) and Mode II (shear). The transition from linear to non-linear behavior begins as soon as the corresponding stress criterion is reached [32]. Up to this point, only elastic strains occur.

$$\left(\frac{\sigma_{t,z}}{f_{t,z}}\right)^2 + \left(\frac{\tau}{f_v}\right)^2 = 1 \tag{5}$$

The fracture, and the complete failure of one cohesive element, is defined in the calculation step where the fracture energy of the cohesive element G^{I} and G^{II} reaches the specific fracture energy of the material G_c^{I} and G_c^{II}. Under combined loading, the failure criterion from Eq. (6) is applied.

$$\left(\frac{G^{I}}{G_c^{I}}\right)^2 + \left(\frac{G^{II}}{G_c^{II}}\right)^2 = 1 \tag{6}$$

By modeling this softening process, stress peaks and stress singularities which often occur in linear elastic FE modeling have less influence on the load-carrying capacity.

2.5. Materials

Solid softwood (SW) and solid beech hardwood (HW) have been used for the timber. The timber was selected as knot-free with mostly radial growth ring orientation in order to avoid premature failure of the timber and, consequently, to generate a comparatively high stress in the adhesively bonded joint. The surfaces of the timber were planed within 24 h before gluing and cleaned of loose parts with compressed air. All timber samples have been stored in constant climate (20 °C, 65% RH) before the tests.

Regarding the prefabricated concrete elements, the strength class C45/55 has been requested with cement type 52,5R and a maximum aggregate diameter of 16 mm. The actual strength class achieved tended to exceed the theoretical average compressive strength class $f_{cm,cube} = 53$ N/mm^2 for C45/55, see Fig. 4. The bottom surface of the concrete elements, which were in contact to the formwork and will be used as gluing surfaces, have either been left smooth (SM) or prepared by different treatments to achieve a rough surface (RH). In the case of smooth concrete surfaces, formwork oils or other release agents have not been allowed and the surfaces have either been left as non-prepared with different formwork materials (NP = concrete formwork panel with phenolic resin film coating, SP = three-ply shuttering panel, OSB = OSB panels) or the concrete has been treated differently, such as utilizing a strong compacting process to artificially let the aggregates sink to the bottom of the prefab near to the gluing surface (CO). In the case of rough concrete surfaces, they have been prepared by either a normal sandblasting (SB2) or a strongly sandblasting process (SB3), by hammering (HA), or treated with hardening retarder (HR) to achieve an exposed aggregate concrete surface.

The structural adhesives, which have been used to bond timber and concrete, are based on two-component epoxy (2EP) or phenol-resorcinol formaldehyde (PRF). Polymer mortars (PM) are based on 2EP adhesives with inert additives as fillers and thixotropy modifiers.

2.6. Material parameters

The most relevant material properties have usually been determined experimentally. Parameters with less influence have been assessed according to available data from the literature. The initial parameters are summarized in this section, while a closer analysis of the shear-strength parameter of the timber will be carried out in Section 4.5 after the calculation methods for the prediction of the failure load are known.

2.6.1. Experimentally determined

The tests described in EN 408 [28] were used for the shear strength of the timber $f_{v,t}$. For the surface tensile strength of the concrete $f_{ct,surf}$, the pull-off test according to DIN 1542 [29] and DIN 1048 [30] have been used. The compression strength of the concrete was determined according to EN 12390-3 [33].

Table 1
Timber — material parameters for the calculation from the literature.

Type of failure criterion	Parameter	Softwood	Source	Hardwood	Source
Stress-based	$f_{t,90,m}$	1.89 N/mm^2	[35]	5.50 N/mm^2	[36]
	$f_{v,t,m}$	6.10 N/mm^2	[37]	11.00 N/mm^2	[38], [39]
	$f_{c,90,m}$	3.24 N/mm^2	[40]	9.60 N/mm^2	[41]
Based on LEFM	$f_{t,z,t}$	$f_{t,90,m}$	–	$f_{t,90,m}$	–
	$f_{v,t}$	$f_{v,t,m}$	–	$f_{v,t,m}$	–
	$G^{I}_{c,t}$	0.30 N/mm	[34]	1.39 N/mm	[42]
	$G^{II}_{c,t}$	$0.23 \cdot f_{v,t,m}$	–	$0.23 \cdot f_{v,t,m}$	–

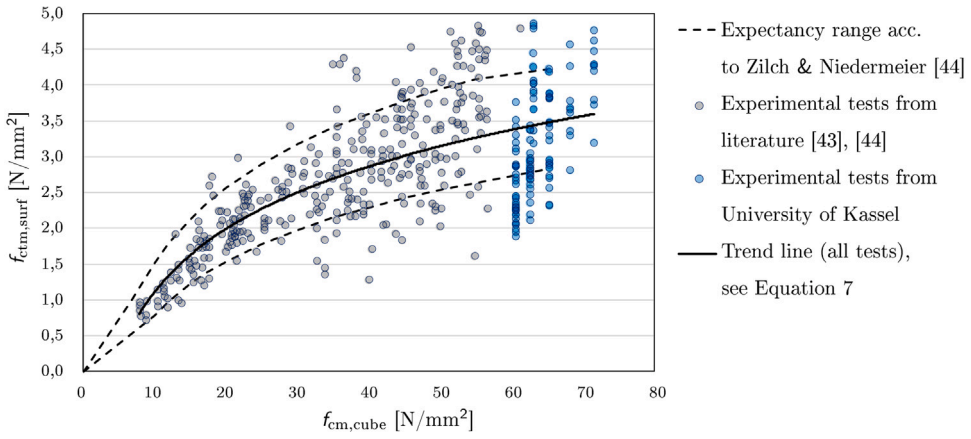

Fig. 4. Relationship between the mean surface tensile strength and concrete compressive strength — literature values and our own experimental data.

Table 2
Concrete — material parameters for the calculation from the literature.

Type of failure criterion	Parameter	Concrete C45/55	Source
Stress-based	$f_{ctm,surf}$	see Eq. (7)	see Fig. 4
Based on LEFM	$f_{t,z,c}$	$f_{ctm,surf}$	–
	$f_{v,t}$	$2 \cdot f_{ctm,surf}$	–
	$G^{I}_{c,c}$	$0.073 \cdot f_{cm}^{0.18}$	[43]
	$G^{II}_{c,c}$	$0.29 \cdot f_{ctm,surf}$	[44]

2.6.2. Supplemented with data from the literature

The material parameters, which have been supplemented from the literature, are summarized in Table 1 and Table 2. No literature values for the specific fracture energy of hardwood in mode II are known to the authors, which is why an estimation must be done. Considering that the fracture parameter f_v and the specific fracture energy G^{II}_c are directly related by the linear cohesive law, modifying f_v exclusively and assuming a constant value for G^{II}_c might not be consistent, although the relationship of shear strength and specific fracture energy in mode II are disputed. Therefore, it has been decided to assess the values based on the results of Jockwer [34], who determines $G^{II}_{c,t} = 1.15$ N/mm for softwood with a shear strength of about $f_{v,t} = 5.0$ N/mm^2, leading to a ratio of $G^{II}_{c,t} = 0.23 \cdot f_{v,t}$ [N/mm].

Eq. (7) is used for the calculation of the concrete's surface tensile strength. This trend line is based on a total of 444 test values from experiments performed at the University of Kassel and experiments from the literature, see Fig. 4.

$$f_{ctm,surf} = 1.29 \cdot ln(f_{cm,cube}) - 1.86 \text{ [N/mm}^2\text{]} \quad (7)$$

2.6.3. Adhesive properties

Referring to Fig. 1, it can be assumed that the bond failure does not occur within the adhesive itself due to the significant disparity in strengths between the adhesive and substrates. This observation is also supported by experimental confirmation (see Fig. 2) as well as a literature review on strength properties of adhesives: Cold-curing epoxy adhesives (2EP) typically exhibit tensile strengths between 25 and 40 N/mm^2 [5,45], while the polymer mortar (PM) used in experiments shows a flexural strength around 40 N/mm^2 [1]. The compressive strength for timber–concrete bonding 2EP adhesives is approximately 84 N/mm^2 [5], whereas PM, due to added aggregates, vary from 90 to 146 N/mm^2 [5]. A PM using a 1.6 mm maximum aggregate size attains 139 N/mm^2 compressive strength [1].

3. Bond specimens

The bond specimens have been tested in several projects at the University of Kassel. A full documentation of all details can be found in the technical reports have been previously published, see Table 3. The original designations used in previously published articles, conference papers, or research reports may differ from those used in this work. A total of 186 test results are available. The test set-up and the ATCC bond specimen as used in test series V1 and V3 are shown in Fig. 5. The same set-up was used for test series V2, with the difference that the concrete part was replaced by polymer mortar. The test set-ups for test series V4, V6 and V7 can be found in Fig. 5 of Frohnmüller et al. [14], for information on test series V5 see Fig. 2 by Frohnmüller et al. [7].

Due to the inclination of the test specimens, the load introduction points at the head and the foot of the specimen align with each other. Cut-ins at the upper and lower ends of the specimens define the bond length of the adhesive precisely and prevent stress concentrations near the load application points. Steel brackets were usually glued onto the timber part of the specimen to improve the load application and achieve a more uniform shear stress distribution. The gluing process was omitted in two cases (V6, V7). The thickness of the adhesive bond was defined using spacers. The thickness of the timber part was adjusted accordingly with varying bond thickness. Typically, two displacement sensors with a ±1 mm measuring range were attached to the upper and lower ends of the specimen to measure the relative displacement. All tests were conducted following the recommended load protocol of EN 26891 [46], with the tests being fully controlled using a constant velocity of 0.01 mm/s. The testing duration for each experiment ranged from four to six minutes. The essential geometries

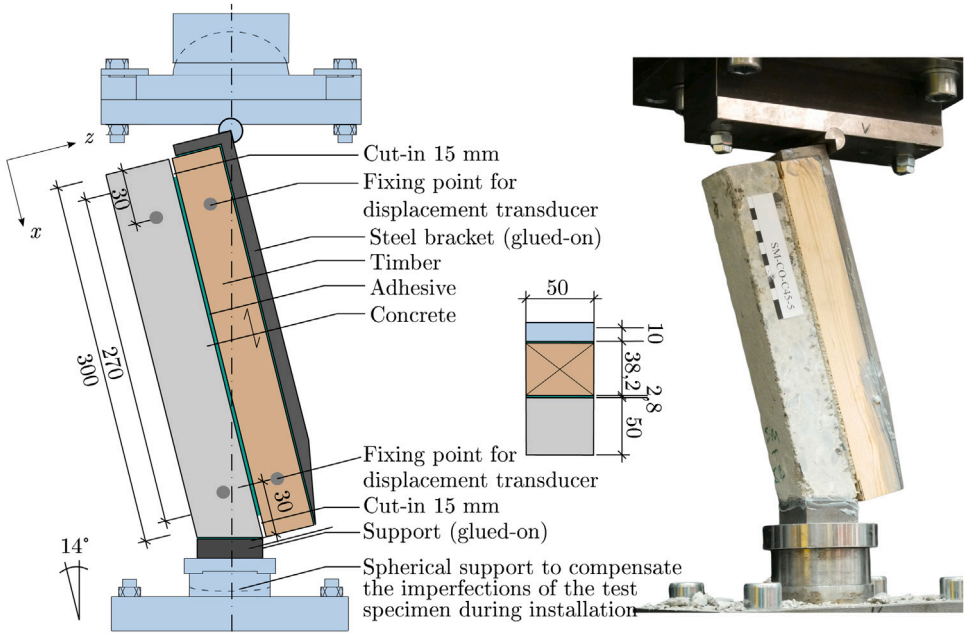

Fig. 5. Typical test set-up and ATCC bond specimen.

Table 3
ATCC bond specimens — Assignment of test series to research projects, scientific publications and technical reports.

Test series	Type of project	Publication
V1	BMWK/ZIM ZF4147005EB9	[47], [1]
V2	Student project, Univ. Kassel	[48]
V3	Service for fischerwerke GmbH	[2]
V4	Student project, Univ. Kassel	[14]
V5	BMWK/ZIM KF2512006KI4	[7]
V6	IGF/AiF 19417 N/282	[14], [8],[12], [49]
V7	IGF/AiF 19417 N/282	*same as V6*

and other parameters required for the calculation and evaluation of the experiments are summarized in Table 4.

4. Prediction of the failure load — methodology

It is necessary to combine a model for stress calculation with a failure criterion and an approach for the analysis of the stresses to predict the failure load for the bond tests in a holistic way. The result is a calculation method for the prediction of the failure load. Based on this literature review from Section 2.2 four calculation methods are chosen in this study:

- An analytical model assuming constant stresses and a consideration of the stress interaction of shear- and normal stresses perpendicular to the bondline (AN)
- A finite element model with linear-elastic material parameters and a consideration of the stress interaction of shear- and normal stresses perpendicular to the bondline (FE-S)
- A finite element model with linear-elastic material parameters and a consideration of the maximum shear stress, so called "peak" (FE-P)
- A non-linear finite element model based on a fracture mechanic approach and cohesive-zone modeling (FE-C)

The calculation methods FE-S and FE-P are based on the same linear-elastic FE model but are different in the post-processing of the stresses and the failure criteria which is applied. While the FE-S calculation method uses the failure criterion to include shear and normal stresses for evaluation, the FE-P calculation method only considers the maximum shear stress value.

The calculation methods are explained in detail below. The results of the calculation for the prediction of the failure load can be found in Section 5 "Validation".

4.1. Analytical (AN)

The bond stresses $\tau_{xz} = \tau$ and σ_z in the AN calculation method are calculated by an analytical approach as a constant stress block depending on the load F, the bond length l_b, the bond width b_b and the angle α, which corresponds to the inclination of the specimen with respect to the load direction.

$$\tau = \frac{F \cdot \cos(\alpha)}{l_b \cdot b_b} \tag{8}$$

$$\sigma_z = \frac{F \cdot \sin(\alpha)}{l_b \cdot b_b} \tag{9}$$

By equating Eq. (8) and Eq. (9), σ_z can be expressed as a function of τ. The relationships for the AN calculation method are shown graphically in Fig. 6 in the shear-normal stress diagram.

$$\sigma_z = \tau \cdot \frac{\sin(\alpha)}{\cos(\alpha)} = \tau \cdot \tan(\alpha) \tag{10}$$

Eqs. (8) and (10) are substituted into Eqs. (2) and (4), then resolved for the failure load (see (11) and (12) in Box I).

The bond failure occurs when the critical failure load $F_{u,cal,b,t}$ or $F_{u,cal,b,c}$ is reached. The stresses τ_u and $\sigma_{z,u}$ correspond with the stresses for the ultimate failure load F_u (see Fig. 6).

$$F_{u,cal,b} = \min \begin{cases} F_{u,cal,b,t} \\ F_{u,cal,b,c} \end{cases} \tag{13}$$

4.2. Linear-elastic FE model with full stress interaction (FE-S)

The calculation method FE-S is based on an ABAQUS 2D-FE model. Linear elastic material parameters are defined because the bond failure observed in experimental studies occurred in all cases in a brittle manner, see Table 5, Table 6 and Table 7. Local axes were considered to account for the anisotropy of the wood. The mesh consists of CPS4R elements with four nodes and an edge length of each element of

Table 4
ATCC bond specimens — Test parameters and number of test specimens.

Test series	b_b [mm]	l_b [mm]	α	Timber	Concrete surface[a]	Adhesive -type	Adhesive -thickness	$F_{u,exp,b,m}$ [kN]	COV [%]	n [–]
V1-01	50	270	14°	SW	SM-NP	PM	3.8 mm	95.0	14	6
-02	50	270	14°	SW	SM-NP	PM	2.0 mm	86.8	11	6
-03	50	270	14°	SW	SM-CO	PM	3.8 mm	91.2	13	6
-04	50	270	14°	SW	RH-HR	PM	3.8 mm	93.5	16	6
-05	50	270	14°	SW	RH-SB3	PM	3.8 mm	91.4	4	6
-06	50	270	14°	SW	RH-HA	PM	3.8 mm	93.3	19	6
V2	50	270	14°	SW	–	PM	51.0 mm	109.3	20	9
V3-01	50	270	14°	SW	SM-NP	2EP	2.0 mm	106.9	12	10
-02	50	270	14°	SW	RH-SB2	2EP	2.0 mm	124.5	6	9
V4-01	25	250	14°	SW	RH-SB2	2EP	1.0 mm	54.4	7	5
	25	250	14°	SW	RH-SB2	PM	5.0 mm	61.8	16	5
	25	250	14°	SW	RH-SB2	PRF	~0.1 mm[a]	45.8	14	5
-02	25	250	14°	SW	SM-NP	2EP	1.0 mm	60.0	12	5
	25	250	14°	SW	SM-NP1	PM	5.0 mm	50.7	14	5
	25	250	14°	SW	SM-NP1	PRF	~0.1 mm[a]	48.3	20	5
-03	25	250	14°	SW	SM-SP	2EP	1.0 mm	47.9	25	5
	25	250	14°	SW	SM-SP	PM	5.0 mm	53.3	10	5
	25	250	14°	SW	SM-SP	PRF	~0.1 mm[a]	53.4	9	5
-04	25	250	14°	SW	SM-OSB	2EP	1.0 mm	47.0	22	5
	25	250	14°	SW	SM-OSB	PM	5.0 mm	49.1	24	5
	25	250	14°	SW	SM-OSB	PRF	~0.1 mm[a]	50.5	3	5
V5-01	80	320	11°	SW[c]	RH-SB2	PM	7.5 mm	109.5	15	9
-02	40	320	11°	SW[c]	RH-SB2	PM	7.5 mm	63.6	8	6
V6-01	50	270	14°	SW	SM-NP	2EP	~0.1 mm[a]	87.3	13	14
-02	50	270	14°	SW	SM-NP	PRF	~0.1 mm[a]	80.2	12	10
-03	50	270	14°	2xSW	–	2EP	~0.1 mm[a]	91.3	6	4
V7-01	50	270	14°	HW	SM-NP	2EP	~0.1 mm[a]	102.8	12	10
-02	50	270	14°	HW	SM-NP	PRF	~0.1 mm[a]	112.2	13	9
								Total number of specimens: 186		

[a] Strength class of the concrete for all test series is C45/55.

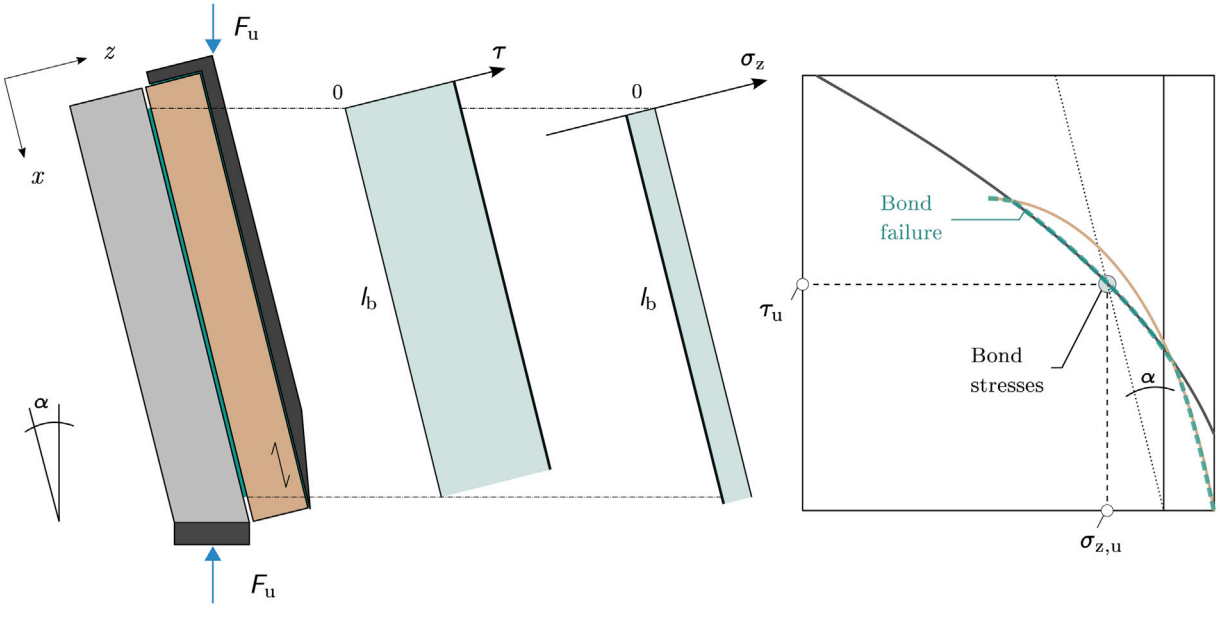

Fig. 6. Calculation method AN — Methodology for the prediction of the failure load, exemplary depicted in the shear–stress- normal stress-diagram for a typical bond test as shown in Fig. 5 and the failure load $F_u = F_{u,cal}$.

$$F_{u,cal,b,c} = \frac{2 \cdot b_b \cdot l_b \cdot f_{ctm,surf}}{1 - \sin(\alpha)} \tag{11}$$

$$F_{u,cal,b,t} = \left(\frac{\sqrt{f_{v,t}^2 \cdot \left(4 \cdot f_{c,90}^2 \cdot f_{t,90}^2 + f_{c,90}^2 \cdot f_{v,t}^2 \cdot \tan^2(\alpha) + 4 \cdot f_{c,90} \cdot f_{t,90}^3 + 2 \cdot f_{c,90} \cdot f_{t,90} \cdot f_{v,t}^2 \cdot \tan^2(\alpha)\right) \cdot \tan^2(\alpha) + f_{t,90}^4}}{(2 \cdot f_{c,90} \cdot f_{t,90} + f_{t,90}^2 + f_{v,t}^2)} \right. \\ \left. \frac{+ f_{t,90}^2 \cdot f_{v,t}^2 \cdot \tan^2(\alpha)} - f_{c,90} \cdot f_{v,t}^2 \cdot \tan(\alpha) \right) \cdot \frac{l_b \cdot b_b}{\cos(\alpha)} \tag{12}$$

Box I.

Table 5
Timber — material parameters for the numerical simulation (mean values).

Timber material	E_x [N/mm²]	E_z [N/mm²]	ν_{xz} [-]	G_{xz} [N/mm²]
Solid wood (SW)	11.000	630	0,45	690
Solid wood (HW)	15.500	1030	0,50	970

Table 6
Concrete — material parameters for the numerical simulation (mean values).

Strength class	E [N/mm²]	ν [-]	G [N/mm²]
C45/55	34.500	0,2	14.375

Table 7
Adhesive — material parameters for the numerical simulation (mean values).

Adhesive	E [N/mm²]	ν [-]	G [N/mm²]
2EP (high viscosity)	4.500	0,4	1.607
2EP (low viscosity)	2.500	0,4	893
PRF	2.500	0,4	893
PM	25.000	0,3	10.500

a_E = 5 mm. The load is applied in the form of a constant vertical displacement at the head of the specimens. The reference point (RP) of the displacement is coupled to the steel bracket and the area of coupling is defined by the contact area of the testing machine with the steel bracket. The load $F_{u,FEM}$ is determined at the reference point at the base of the specimen, which is coupled with the steel plate.

It is assumed in the calculation method (FE-S) that all bond stress pairs $\tau_{i,FE}$, $\sigma_{z,i,FE}$ along the bondline can be decisive for the bond failure. Therefore, the shear stress $\tau_{i,FE}$ and the normal stresses in the local z-direction $\sigma_{z,i,FE}$ were calculated for each FE node i along the selected path in the FE model, see Fig. 7. The path is located parallel to the adhesive joint within the first row of FE elements in the respective substrate and, thus, matches the actual fracture surfaces as observed in the tests (see Fig. 2).

The bond stress pairs are then formulated with reference to the FE model load F_{FE} to predict the failure load $F_{u,i}$. Due to the linear-elastic material model, the bond stresses from the FE calculation can be linearly scaled. It is helpful for the further calculation steps that at this point the substitution variables t_i=($\tau_{i,FE}/F_{FE}$) and s_i=($\sigma_{z,i,FE}/F_{FE}$) are introduced.

$$\tau_{u,i} = \tau_{i,FE} \cdot \frac{F_{u,i}}{F_{FE}} = F_{u,i} \cdot t_i \tag{14}$$

$$\sigma_{z,u,i} = \sigma_{z,i,FE} \cdot \frac{F_{u,i}}{F_{FE}} = F_{u,i} \cdot s_i \tag{15}$$

In a next step, the stress components $\tau_{u,i}$ and $\sigma_{z,u,i}$ (Eq. (14) and Eq. (15)) are inserted into the equations of the failure criteria.

The failure criterion from Eq. (4) is used analogously to the AN calculation method for concrete. When rearranged according to the force, the failure load $F = F_{u,cal,b,c,i}$ can be calculated for each bond stress pair along the evaluation path, see Eq. (16).

$$F_{u,cal,b,c,i} = \frac{2 \cdot (\sqrt{f_{ctm,surf}^2 \cdot (s_i^2 + t_i^2)} - f_{ctm,surf} \cdot s_i)}{t_i^2} \tag{16}$$

The failure criterion from Eq. (2) is used with a modified application limit in the compression–shear range for timber. In order to calculate the failure load, Eq. (3) is resolved by the force $F = F_{u,cal,b,t,i}$.

$$F_{u,cal,b,t,i} = \frac{\sqrt{f_v^2 \cdot (4t_i^2 \cdot f_{c,90}^2 \cdot f_{t,90}^2 + 4 \cdot t_i^2 \cdot f_{c,90} \cdot f_{t,90}^3 + t_i^2 \cdot f_{t,90}^4 + s_i^2 \cdot f_{c,90}^2 \cdot f_v^2}}{2 \cdot t_i^2 \cdot f_{c,90} \cdot f_{t,90} + t_i^2 \cdot f_{t,90}^2 + s_i^2 \cdot f_v^2} \\ \frac{+2 \cdot s_i^2 \cdot f_{c,90} \cdot f_{t,90} \cdot f_v^2 + s_i^2 \cdot f_{t,90}^2 \cdot f_v^2)} - s_i \cdot f_{c,90} \cdot f_v^2}{} \quad \text{for } \sigma_z \le f_{c,90} \tag{17}$$

$$F_{u,cal,b,t,i} = \frac{\sqrt{f_v^2 \cdot f_{c,90}^2 + 2 \cdot f_v^2 \cdot f_{c,90} \cdot f_{t,90} + f_v^2 \cdot f_{t,90}^2}}{2 \cdot t_i^2 \cdot f_{c,90} \cdot f_{t,90} + t_i^2 \cdot f_{t,90}^2} \quad \text{for } \sigma_z > f_{c,90} \tag{18}$$

The governing failure load $F_{u,cal,b}$ corresponds to the smallest value of the calculated failure loads $F_{u,cal,b,t}$ and $F_{u,cal,b,c}$.

$$F_{u,cal} = \min \begin{cases} F_{u,cal,b,t} = \min(F_{u,cal,b,t,1}, F_{u,cal,b,t,2}, \dots, F_{u,cal,b,t,i}) \\ F_{u,cal,b,c} = \min(F_{u,cal,b,c,1}, F_{u,cal,b,c,2}, \dots, F_{u,cal,b,c,i}) \end{cases} \tag{19}$$

4.3. Linear-elastic FE model with shear stress peak (FE-P)

The FE-P calculation method is based on the same finite element model as the FE-S calculation method, with the difference that for FE-P, it is assumed that only the maximum value, i.e., the peak of the shear stresses, governs the bond failure.

The respective maximum shear stress values from Eq. (14) for concrete $\tau_{c,FE,max}$ and timber $\tau_{t,FE,max}$ are then substituted into the shear strength failure criterion from Eq. (1), and the failure load is solved accordingly. This results in Eq. (20) for the concrete and Eq. (21) for the timber. The governing failure load $F_{u,cal,b}$ is then determined as the minimum of $F_{u,cal,b,c}$ and $F_{u,cal,b,t}$.

$$F_{u,cal,b,c} = F_{FE} \cdot \frac{f_{v,c}}{\tau_{c,FE,max}} \tag{20}$$

$$F_{u,cal,b,t} = F_{FE} \cdot \frac{f_{v,t}}{\tau_{t,FE,max}} \tag{21}$$

$$F_{u,cal,b} = \min \begin{cases} F_{u,cal,b,c} \\ F_{u,cal,b,t} \end{cases} \tag{22}$$

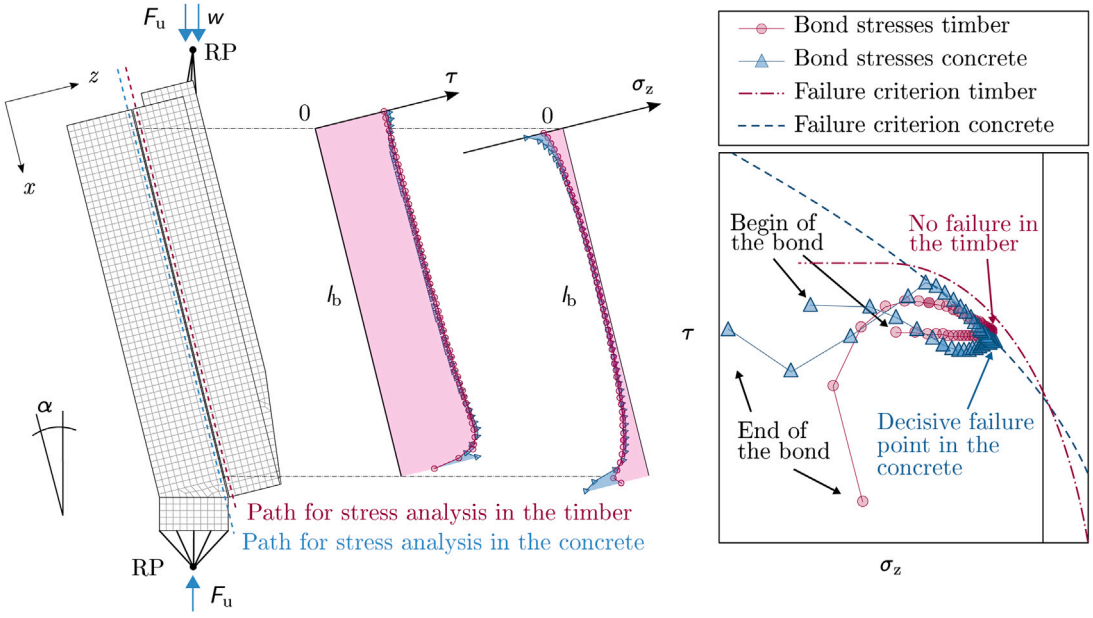

Fig. 7. Calculation method FE-S — Methodology for the prediction of the failure load, exemplarily depicted in the shear-normal stress diagram for a typical bond test as shown in Fig. 5 and the failure load $F_u = F_{u,cal}$.

4.4. Non-linear FE model with cohesive zones (FE-C)

A numerical method for implementing a LEFM method is the Cohesive Zone Model (CZM), where the crack is represented as the cohesive failure of individual FE elements. The cohesive zone is assigned all the non-linear properties of the crack process, while the surrounding material exhibits linear-elastic behaviour. This makes the CZM particularly suitable when the location and direction of the crack are known, which is the case for adhesive bondlines (see Fig. 2). The calculation method FE-C is implemented using the FE software ABAQUS, where two cohesive zones are arranged, with one assigned the calculation parameters of the timber and the other assigned the calculation parameters of the concrete, see Fig. 8.

Once the stress criterion of Eq. (5) is met, damage is initiated and the cohesive element begins to soften. The softening is described numerically by the damage parameter D.

$$D = \frac{\delta_m^1(\delta_m^{max} - \delta_m^0)}{\delta_m^{max}(\delta_m^1 - \delta_m^0)} \tag{23}$$

When $D = 0$, the cohesive element is intact. When D reaches a value of 1, complete softening is achieved. The parameter δ_m^0 corresponds to the effective deformation at the beginning of the crack, δ_m^1 at the end of the crack, where δ_m is composed of the deformation components from Mode I ($\delta_{t,z}$) and Mode II (δ_v), see Eq. (24).

$$\delta_m = \sqrt{\delta_{t,z}^2 + \delta_v^2} \tag{24}$$

The effect that a crack cannot reharden is considered through the definition of the parameter δ_m^{max}. This parameter corresponds to the deformation that the finite element experiences under the applied load until the iteration step considered. Under linearly increasing loading, δ_m^{max} corresponds to the deformation δ_m. If the loading is reduced again, δ_m will decrease, but the value of δ_m^{max} remains constant.

Furthermore, the definition of the cohesive law modifies the stresses occurring on the cohesive zone element through the damage parameters D. As a consequence, the tensile stresses $\sigma_{t,z}$ cannot exceed the predefined strength parameters $f_{t,z}$ and f_v at any time and stress peaks or singularities are, thus, prevented. A linear cohesive law is applied, which has proven to be effective in describing cohesive failure of a notched pin joint under combined shear–tensile loading in Claus' investigations [32]. The parameters $\bar{\sigma}_{t,z}$ and $\bar{\tau}$ represent the stress components without considering the damage. The bond failure occurs when the failure criterion of Eq. (6) is reached.

$$\text{Cohesive law mode I: } \sigma_{t,z} = \begin{cases} (1-D)\bar{\sigma}_{t,z} & \text{for } \sigma_{t,z} \geq 0 \\ \bar{\sigma}_{t,z} & \text{for } \sigma_{t,z} < 0 \end{cases} \tag{25}$$

$$\text{Cohesive law mode II: } \tau = (1-D)\bar{\tau} \tag{26}$$

4.5. Analysis of material properties considering the calculation method

The strength parameters for the calculation methods have a significant influence on the prediction as they directly affect the failure criterion. Typically, the standard that describes the test set-up for the strength parameter also includes an (often analytical) approach to calculate the strength parameters based on the failure load, as given in EN 408 [28] for the shear strength of the timber $f_{v,t,n}$, for example, see Eq. (27).

$$f_{v,t,n} = \frac{F_{u,exp} \cdot cos(\alpha)}{l_t \cdot b_t} \tag{27}$$

The question arises, however, if higher accuracy in the subsequent prediction of the bond specimen's failure load could be achieved by consistently applying the same calculation methods for the determination of strength parameters from the preliminary tests. When the shear test from EN 408 [28] is analysed using the FE-S and FE-P calculation methods, the strength parameter obtained deviates from the normative value $f_{v,t,n}$. The normative value for a sample failure load in the test of $F_{u,exp} = 60.4$ kN would result in $f_{v,t,n} = 6.10$ N/mm^2. However, when using the FE-S numerical calculation method, the value increases to $f_{v,t,FE\text{-}S} = 7.22$ N/mm^2, as shown in Fig. 9. The critical shear path for the calculation method FE-S is located in the middle of the test specimen, while it is at the edge of the specimen parallel to the bonded steel bracket for the calculation method FE-P. The shear flow, however, remains the same for both methods.

Therefore, the mean shear strength $f_{v,t,m}$ can be expressed with factors related to the shear strength parameter $f_{v,t,n}$ calculated according to EN 408, see Table 8.

Regarding the literature, similar approaches can be found in the work of Glasner et al. [50], where the rolling shear strength of timber was determined using the same calculation method for obtaining

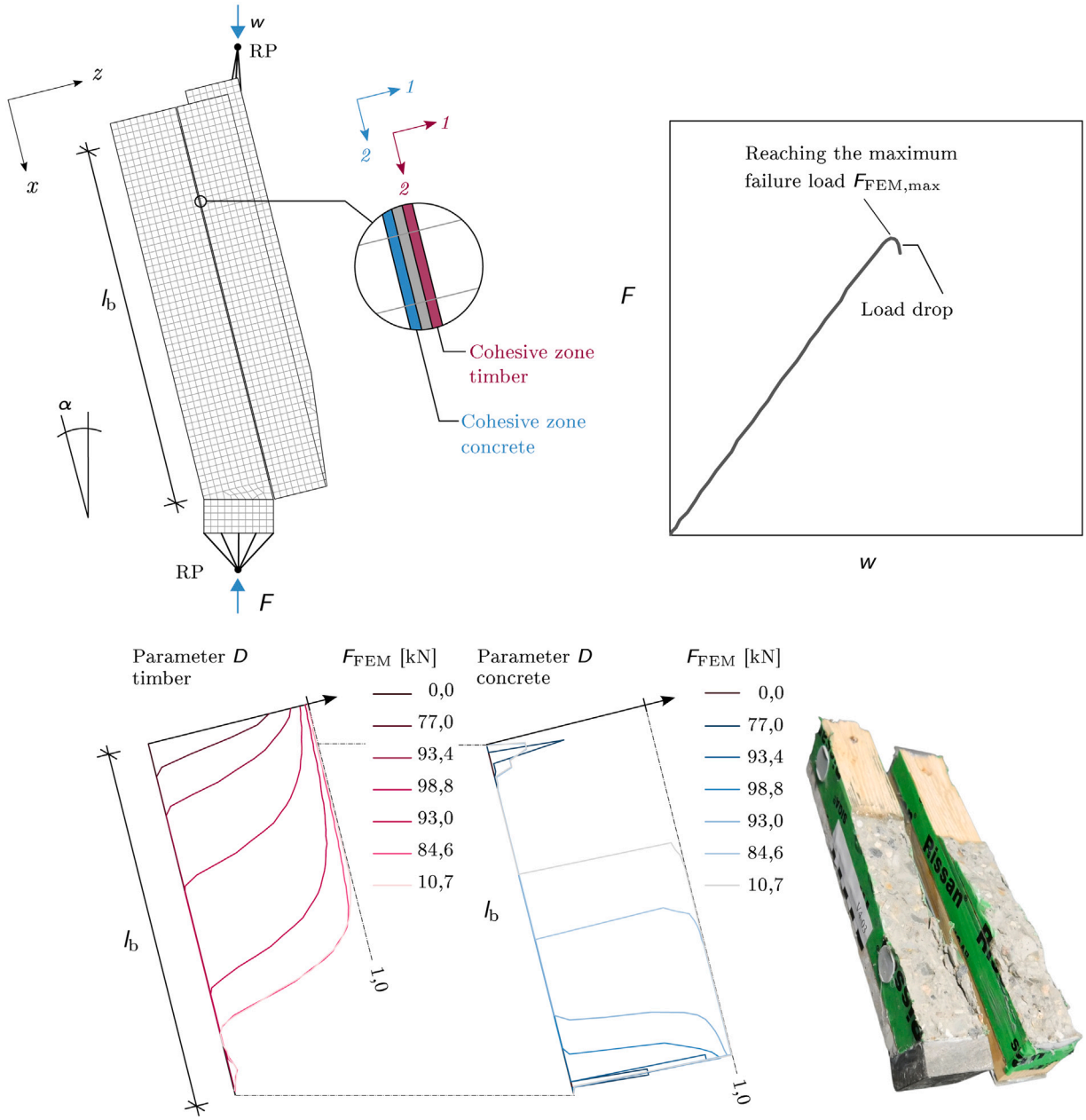

Fig. 8. Calculation method FE-C — Methodology for the prediction of the failure load, exemplarily depicted in the load–displacement diagram and development of the damage parameter D with exemplarily related crack surface of bond test V3-01.

Table 8
Modified, shear strength $f_{v,t}$ for the calculation methods.

Calculation method	$f_{v,t}$ [N/mm^2]	
	Softwood	Beech
AN	$1.00 \cdot f_{v,t,n}$	$1.00 \cdot f_{v,t,n}$
FE-S	$1.18 \cdot f_{v,t,n}$	$1.18 \cdot f_{v,t,n}$
FE-P	$1.42 \cdot f_{v,t,n}$	$1.51 \cdot f_{v,t,n}$

strength parameters as used in the later prognosis. Akter et al. [25] also suggest a combination of experimental investigations and numerical calculations to determine the strength parameters for the later-used failure criterion. In the following, this approach is applied for determining the strength parameter of the shear strength of the timber. The standardized proposed determination of the calculation parameters is used for the strength parameters with pure tensile stress ($f_{t,90}$, $f_{ct,surf}$) or pure compressive stress ($f_{c,90}$).

The initial parameters $G_{c,t}^{II}$ and $f_{v,t}$ must be selected in a first step for an in-depth analysis of the fracture parameters of the timber with the calculation method FE-C. The value given by Jockwer et al. [34] was used, which was determined for a mixed sample of solid wood and glued laminated timber and can be regarded as particularly suitable due to the large number of tests on the specific fracture energy of softwood. Due to the sample of mixed-quality timber, the shear strength associated with the specific fracture energy consequently corresponds to the mean value $f_{v,t,m} = 5,0$ N/mm^2 of the shear strength of solid softwood according to Glos & Denzler [51] ($f_{v,t,m} = 4,0$ N/mm^2) and glued laminated timber according to Schickhofer [52] ($f_{v,t,m} = 6,1$ N/mm^2).

Regarding the shear strength, the same value $f_{v,t,m} = 6.1$ N/mm^2 as for the FE-S calculation method is used as the initial parameter for

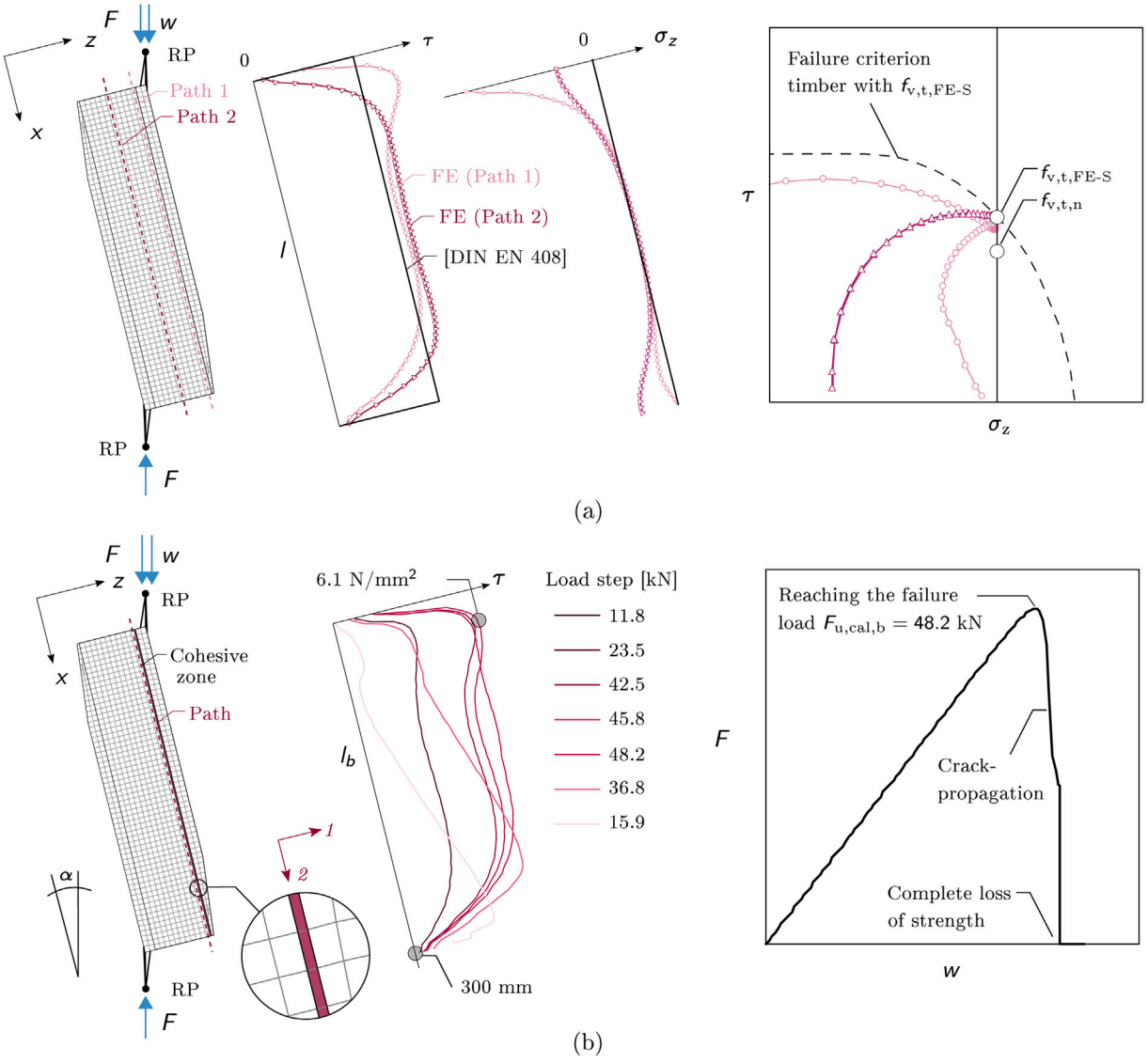

Fig. 9. Determination of the strength parameter $f_{v,t}$ with the shear test acc. to EN 408 (a) FE-S (b) FE-C (parameters acc. to Table 9).

Table 9
Initial parameters for the cohesive zone in the FE-C calculation method for modelling the shear test according to [28].

Wood type	E_t	G_t	$f_{t,z}$	$f_{v,t}$	$G_{c,t}^{I}$	$G_{c,t}^{II}$
	[N/mm²]				[N/mm]	
Softwood	630	690	1.89	6.10	0.30	1.40
Beech	1030	970	5.50	11.00	1.39	2.53

Table 10
Modified fracture parameters in mode II — calculation method FE-C.

Wood type	$f_{v,t}$ [N/mm²]	$G_{c,t}^{II}$ [N/mm]
Softwood	$1.25 \cdot f_{v,t,m,n}$	$0.23 \cdot f_{v,t}$
Beech	$1.36 \cdot f_{v,t,m,n}$	$0.23 \cdot f_{v,t}$

the in-depth analysis of the FE-K calculation method for reasons of comparability. Given that the fracture parameter f_v and the specific fracture energy G_c^{II} are directly related by the linear cohesive law, modifying only f_v while assuming a constant value for G_c^{II} may not be consistent. Therefore, the specific fracture energy $G_{c,t}^{II}$ is modified similarly as f_v. The parameters of the cohesive zone, which are initially chosen based on the literature data, are summarized in Table 9.

The result of the model with the parameters of Table 9 is a failure load of $F_{u,cal,b} = 48.2$ kN, see Fig. 9. With the knowledge of this failure load and the load $F_{u,exp,n} = 60.4$ kN, which theoretically should be present for the strength parameter $f_{v,t} = 6.10$ N/mm² used, a difference can be observed. This finding stands in line with Eisenhut's research [11], where a similar difference of 20% is evident when comparing the failure load calculated using the cohesive zone model with the theoretical failure load according to EN 408. Rahman et al. [53] also found a similar trend in their study of Mode-II specimens, where specimens with an adhesive bondline exhibited about 20% higher specific fracture energy compared to specimens made entirely of solid timber without any adhesive bond. Regarding this study, this means that the parameters underlying the calculation need to be increased until the condition $F_{u,exp,n} = F_{u,cal,b} = 60.4$ kN is met. Accordance between $F_{u,exp,n}$ and $F_{u,cal,b}$ is observed when both fracture parameters were increased by 25% for softwood and 36% for beech, see Table 10.

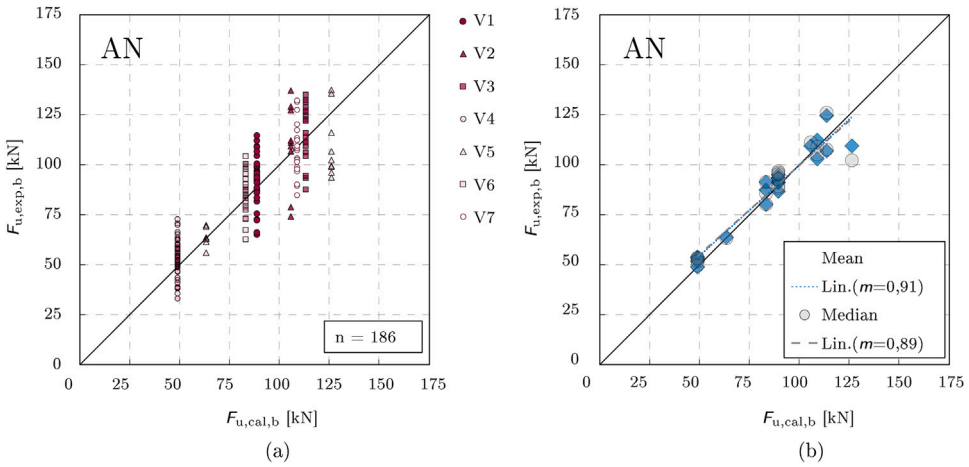

Fig. 10. Results — Comparison of the predicted and calculated failure load for the calculation method AN, FE-S and FE-P (a) All test values (b) Mean and median.

5. Validation

5.1. Results — Comparison of prediction and experiment

The results of the calculation methods are shown in Fig. 10 and Fig. 11. The individual values and the strength parameters underlying the failure criteria are summarized in Tables 11–14. Since the AN calculation method does not include a Young's modulus in the prediction equations but only geometric quantities, some test series (e.g. test series V4) can be combined.

Overall, there is a good agreement between the predictions and the experimental results. Both the mean and the median of the linear regression lines ("Lin".) are close to the bisector for AN. The gradient of the trend lines is $m = 0.91$ for the mean and $m = 0.89$ for the median, which corresponds to a deviation of about 10% from the ideal gradient of $m = 1.00$.

The experimental results for FE-S indicate slightly higher failure loads than predicted. The trend line of the experimental data lies above the bisector with a gradient of $m = 0.93$ for the mean and $m = 0.92$ for the median. The deviation between calculation and experiment decreases slightly with increasing failure load.

The deviation between prediction and experiment for FE-P is noticeably larger than the previous calculation methods AN and FE-S. However, the gradient of the regression line is nearly parallel to the bisector with a value of $m = 1.02$.

The experimental results for FE-C are slightly underestimated on average. The regression line of the experimental data, similar to the FE-S and FE-P calculation methods, lies above the bisector with a gradient of $m = 1.16$ for the mean and $m = 1.15$ for the median. The deviation between calculation and experiment tends to increase with larger failure loads.

5.2. Further observations

Further observations are that the type of failure documented in the tests agrees with the prediction. This becomes evident exemplarily in the shear-normal stress diagram, exemplified for test series V1 in Fig. 12a and for test series V5 in Fig. 12b. When constructing the failure criterion for bond failure, it is noteworthy that the curves of test series V1-01 are relatively close to each other, while in test series V5, the concrete clearly governs the failure behavior.

Regarding FE-S, the FE model and the bond stresses for the test series V7 are depicted in Fig. 13. The fact that the steel bracket is not glued but only placed loosely on the bond specimens was considered in the FE model by defining friction coefficients of $\eta = 0.5$ for the steel–timber contact condition and $\eta = 0.4$ for the steel–concrete contact condition. The modeling of the friction results in the main force being transmitted through contact in the upper region of the specimen. The steel bracket lifts off from the timber in the lower region of the specimen, and a relative displacement between the concrete part and the steel support in the top-left corner can also be seen. This results in an uneven distribution of shear stresses in the adhesive zone compared to the tests with glued steel brackets, which also becomes evident in the shear-normal stress diagram shown in Fig. 13. The failure is primarily influenced by a combination of shear and compressive stresses in the concrete.

6. Conclusions

6.1. Bond strength

Based on the results, it can be observed that the AN calculation method provides a quick and robust approach for predicting the bond failure of ATCC specimens. Despite the comparatively rough assumption of constant bond stresses along the adhesive joint, the experimental results are neither significantly overestimated nor underestimated. The FE-S calculation method, where the non-linear distribution of shear and normal stresses perpendicular to the joint along the adhesive joint are considered, also yields satisfactory results. The FE-P calculation method, which considers only the shear stress peak and neglects normal stresses, leads to an earlier attainment of the failure criterion compared to FE-S and results in a stronger underestimation of the experimental results. The FE-K calculation method allows for a more accurate representation of the failure processes compared to the other methods, but it also tends to underestimate the experimental results and can, therefore, be assessed as conservative.

Furthermore, the results indicate that the agreement between calculation methods and experimental results is not dependent on the magnitude of the failure load, as the gradient of the regression lines for AN and FE-S tends to decrease (m < 1.00), while it increases for FE-P and FE-C ($m > 1.00$). Thus, it can be said that the agreement between prediction and experiment is more influenced by the calculation method than the load level. Similar can be found regarding a potential effect of the bond length, where no clear trend could be observed. Test series with shorter bond lengths, such as V4 ($l_b = 250$ mm), show a similar agreement with the predicted failure load as test series with longer bond lengths, for example, V1, V3 ($l_b = 270$ mm), and V5-02 ($l_b = 320$ mm). The same holds true for a potential bond width effect, except for the individual test series V5-01 ($b_b = 80$ mm), where the experimental results tend to be underestimated compared to the prediction. Considering the agreement between test series V4 ($b_b =$

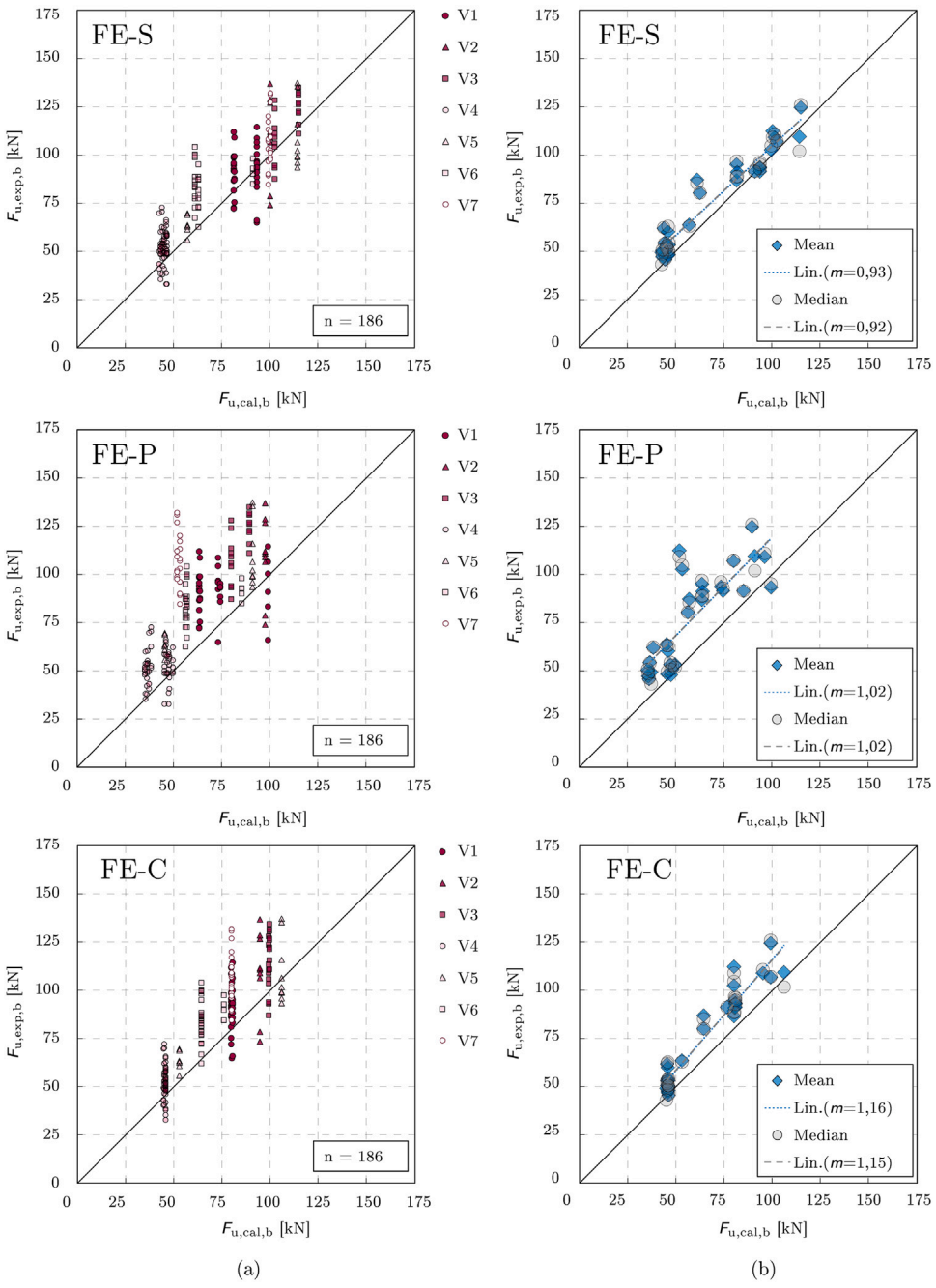

Fig. 11. Results — Comparison of the predicted and calculated failure load for the calculation method FE-C (a) All test values (b) Mean and median.

25 mm) and V5-02 (b_b = 40 mm), as well as test series V1, V2, V3, V6, and V7 (b_b = 50 mm), no bond width effect is evident.

6.2. Test methodology/testing procedure

The testing methodology for ATCC specimens differs fundamentally from the approach used for mechanical connections, such as bolts, screws, and notches. While the primary focus in mechanical connections is on experimentally determining the connector stiffness, denoted as K_{ser}, for adhesive connections, the emphasis shifts towards evaluating the functionality and adhesion properties of the adhesive. When structural adhesives with a high modulus of elasticity and a high shear strength, such as polymer mortars or highly filled epoxy adhesives, are being used, a full bond can usually be assumed from the start. Consequently, the bond failure can be clearly attributed to the strength of the substrate materials — timber and concrete. Therefore, the testing methodology should focus primarily on questions related to the overall suitability of the adhesive, the associated application technique, and the prevention of premature adhesion failure.

Before conducting bond tests, it is strongly recommended to ensure that the essential material properties necessary for predicting the failure load are known. In particular, the concrete's pull-off test is crucial for determining its surface tensile strength, while information regarding the properties of timber can usually be obtained from standards and literature. With these strength parameters in hand, it becomes possible to predict the failure load for a bond failure. Subsequently, the experimental failure load obtained from the test can be used to validate the prediction method. An additional advantage of employing the surface

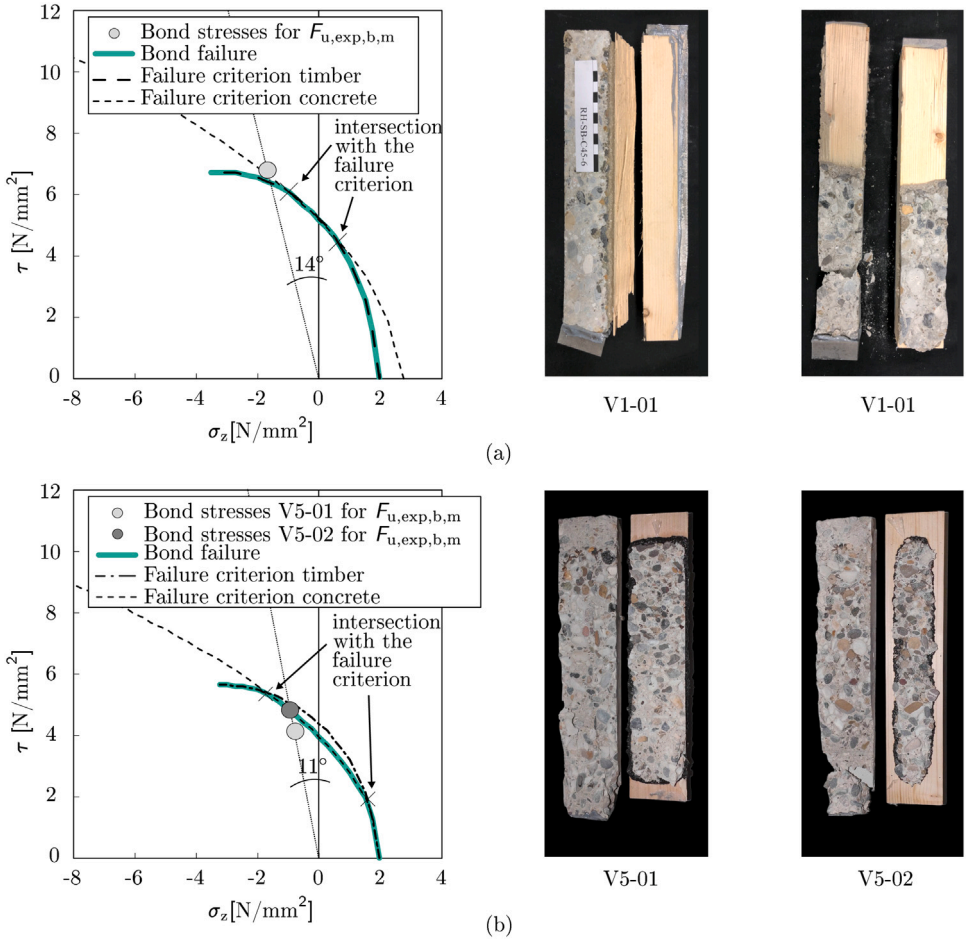

Fig. 12. Results of the calculation method AN in the shear-normal stress diagram and corresponding failure modes (a) Test series V1-01 (b) Test series V5-01 and V5-02.

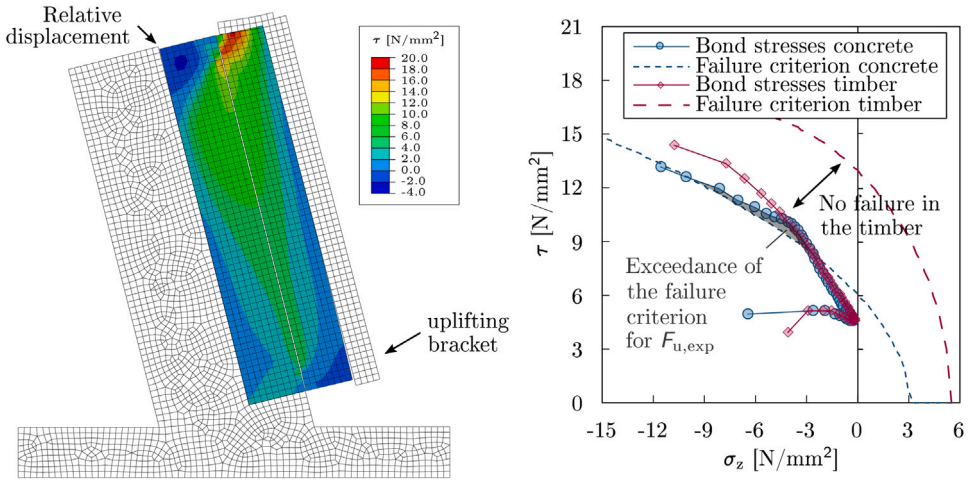

Fig. 13. Results of calculation method FE-S in an abaqus visualization and in the shear-normal stress diagram for the experimental failure load $F_{u,exp}$ for the test series V7.

Table 11
Predicted failure load and related strength parameters — Calculation method AN.

Test series		$F_{u,exp,b,m}$	Strength parameters [N/mm²][a]				$F_{u,cal,b}$ [kN][b]	
		[kN]	$f_{t,90,m}$	$f_{v,m}$	$f_{c,90,m}$	$f_{ctm,surf}$	$F_{u,cal,b,t}$	$F_{u,cal,b,c}$
V1	-01	95.0	*1.89*	5.24	*3.24*	2.59	**89.0**	95.0
	-02	86.8	*1.89*	5.24	*3.24*	2.59	**89.0**	86.8
	-03	91.2	*1.89*	5.24	*3.24*	2.60	**89.0**	92.6
	-04	93.5	*1.89*	5.24	*3.24*	2.98	**89.0**	106.1
	-05	91.4	*1.89*	5.24	*3.24*	3.03	**89.0**	107.9
	-06	93.3	*1.89*	5.24	*3.24*	4.16	**89.0**	148.2
V2		109.3	*1.89*	*6.10*	*3.24*	–	**105.5**	–
V3	-01	106.9	*1.89*	6.50	*3.24*	3.25	**113.2**	115.8
	-02	124.5	*1.89*	6.50	*3.24*	3.64	**113.2**	129.6
V4	-01	54.0	*1.89*	*6.10*	*3.24*	3.25	**48.8**	53.6
	-02	53.0	*1.89*	*6.10*	*3.24*	4.07	**48.8**	67.1
	-03	51.5	*1.89*	*6.10*	*3.24*	4.20	**48.8**	69.3
	-04	48.9	*1.89*	*6.10*	*3.24*	3.16	**48.8**	52.1
V5	-01	109.5	*1.89*	4.40	*3.24*	1.99	132.9	**125.9**
	-02	63.6	*1.89*	4.40	*3.24*	1.99	66.5	**63.0**
V6	-01	84.4	*1.89*	4.93	*3.24*	3.05	**83.1**	108.6
	-02	84.4	*1.89*	4.93	*3.24*	3.05	**83.1**	108.6
	-03	91.3	*1.89*	4.93	*3.24*	–	**83.1**	–
V7	-01	107.2	*5.50*	*11.00*	*9.60*	3.05	179.7	**108.6**
	-02	107.2	*5.50*	*11.00*	*9.60*	3.05	179.7	**108.6**

[a] Italicized values were assumed based on data from relevant literature sources.
[b] The decisive failure load $F_{u,cal,b} = \min(F_{u,cal,b,t}; F_{u,cal,b,c})$ is highlighted.

Table 12
Predicted failure load and related strength parameters — Calculation method FE-S.

Test series			$F_{u,exp,b,m}$	Strength parameters [N/mm²][a]				$F_{u,cal,b}$ [kN][b]	
			[kN]	$f_{t,90,m}$	$f_{t,v,m}$	$f_{c,90,m}$	$f_{ctm,surf}$	$F_{u,cal,b,t}$	$F_{u,cal,b,c}$
V1	-01		95.0	*1.89*	1.18·5.24	*3.24*	2.59	93.7	**81.7**
	-02		86.8	*1.89*	1.18·5.24	*3.24*	2.59	93.7	**81.7**
	-03		91.2	*1.89*	1.18·5.24	*3.24*	2.60	93.7	**82.1**
	-04		93.5	*1.89*	1.18·5.24	*3.24*	2.98	**93.7**	94.0
	-05		91.4	*1.89*	1.18·5.24	*3.24*	3.03	**93.7**	95.6
	-06		93.3	*1.89*	1.18·5.24	*3.24*	4.16	**93.7**	131.3
V2			109.3	*1.89*	1.18·*6.10*	*3.24*	–	**101.5**	–
V3	-01		106.9	*1.89*	1.18·6.50	*3.24*	3.25	115.3	**102.6**
	-02		124.5	*1.89*	1.18·6.50	*3.24*	3.64	115.3	**114.9**
V4	-01	2EP	54.4	*1.89*	1.18·*6.10*	*3.24*	3.25	46.2	**44.5**
		PM	61.8	*1.89*	1.18·*6.10*	*3.24*	3.25	45.3	**43.9**
		PRF	45.8	*1.89*	1.18·*6.10*	*3.24*	3.25	46.4	**44.6**
	-02	2EP	60.0	*1.89*	1.18·*6.10*	*3.24*	4.07	**46.2**	55.7
		PM	50.7	*1.89*	1.18·*6.10*	*3.24*	4.07	**45.3**	55.0
		PRF	48.3	*1.89*	1.18·*6.10*	*3.24*	4.07	**46.4**	55.8
	-03	2EP	47.9	*1.89*	1.18·*6.10*	*3.24*	4.20	**46.2**	57.5
		PM	53.3	*1.89*	1.18·*6.10*	*3.24*	4.20	**45.3**	56.7
		PRF	53.4	*1.89*	1.18·*6.10*	*3.24*	4.20	**46.4**	57.6
	-04	2EP	47.0	*1.89*	1.18·*6.10*	*3.24*	3.16	46.2	**43.3**
		PM	49.1	*1.89*	1.18·*6.10*	*3.24*	3.16	45.3	**42.7**
		PRF	50.5	*1.89*	1.18·*6.10*	*3.24*	3.16	46.4	**43.4**
V5	-01		109.5	*1.89*	1.18·4.40	*3.24*	1.99	141.4	**114.3**
	-02		63.6	*1.89*	1.18·4.40	*3.24*	1.99	70.7	**57.1**
V6	-01		84.4	*1.89*	1.18·4.93	*3.24*	3.05	**61.1**	112.4
	-02		84.4	*1.89*	1.18·4.93	*3.24*	3.05	**62.8**	119.9
	-03		91.3	*1.89*	1.18·4.93	*3.24*	–	**91.3**	–
V7	-01		102.8	*5.50*	1.18·*11.00*	*9.60*	3.05	112.4	**99.4**
	-02		112.2	*5.50*	1.18·*11.00*	*9.60*	3.05	118.8	**100.4**

[a] Italicized values were assumed based on data from relevant literature sources.
[b] The decisive failure load $F_{u,cal,b} = \min(F_{u,cal,b,t}; F_{u,cal,b,c})$ is highlighted.

tensile strength of the concrete as a strength parameter is that it can be assessed directly on the construction site using the bond pull-off test as part of potential quality assurance measures.

An essential next step in the experimental methodology for ATCC is the performance of full-scale bending tests. These tests serve both to validate the insights from the bond experiments and verify whether the adhesive system is capable of compensating for irregularities between scaled timber sections and concrete slabs, establishing continuous contact between timber and concrete. On this scale, it is further possible to assess whether the gluing technique is robust and fulfills the requirements from an economic perspective.

Table 13
Predicted failure load and related strength parameters — Calculation method FE-P.

Test series			$F_{u,exp,b,m}$	Strength parameters [N/mm²][a]		$F_{u,cal,b}$ [kN][b]	
			[kN]	$f_{v,t,m}$	$f_{v,c,m}$	$F_{u,cal,b,t}$	$F_{u,cal,b,c}$
V1	-01		95.0	1.42·5.24	2.0·2.59	99.4	**63.8**
	-02		86.8	1.42·5.24	2.0·2.59	99.4	**63.8**
	-03		91.2	1.42·5.24	2.0·2.60	99.4	**64.0**
	-04		93.5	1.42·5.24	2.0·2.98	99.4	**73.4**
	-05		91.4	1.42·5.24	2.0·3.03	99.4	**74.6**
	-06		93.3	1.42·5.24	2.0·4.16	**99.4**	102.5
V2			109.3	1.42·*6.10*	–	**96.4**	–
V3	-01		106.9	1.42·6.50	2.0·3.25	123.3	**80.0**
	-02		124.5	1.42·6.50	2.0·3.64	123.3	**89.6**
V4	-01	2EP	54.4	1.42·*6.10*	2.0·3.25	48.7	**36.9**
		PM	61.8	1.42·*6.10*	2.0·3.25	50.0	**38.5**
		PRF	45.8	1.42·*6.10*	2.0·3.25	48.6	**36.5**
	-02	2EP	60.0	1.42·*6.10*	2.0·4.07	48.7	**46.2**
		PM	50.7	1.42·*6.10*	2.0·4.07	50.0	**48.2**
		PRF	48.3	1.42·*6.10*	2.0·4.07	48.6	**45.7**
	-03	2EP	47.9	1.42·*6.10*	2.0·4.20	48.7	**47.6**
		PM	53.3	1.42·*6.10*	2.0·4.20	50.0	**49.8**
		PRF	53.4	1.42·*6.10*	2.0·4.20	48.6	**47.1**
	-04	2EP	47.0	1.42·*6.10*	2.0·3.16	48.7	**35.8**
		PM	49.1	1.42·*6.10*	2.0·3.16	50.0	**37.4**
		PRF	50.5	1.42·*6.10*	2.0·3.16	48.6	**35.5**
V5	-01		109.5	1.42·4.40	2.0·1.99	141.3	**90.9**
	-02		63.6	1.42·4.40	2.0·1.99	70.6	**45.5**
V6	-01		84.4	1.42·4.93	2.0·3.05	57.21	**57.2**
	-02		84.4	1.42·4.93	2.0·3.05	58.8	**56.6**
	-03		91.3	1.42·4.93	–	**85.4**	–
V7	-01		102.8	1.42·*11.00*	2.0·3.05	139.6	**53.5**
	-02		112.2	1.42·*11.00*	2.0·3.05	147.7	**52.0**

[a] Italicized values were assumed based on data from relevant literature sources.
[b] The decisive failure load $F_{u,cal,b} = \min(F_{u,cal,b,t}; F_{u,cal,b,c})$ is highlighted.

Table 14
Predicted failure load and related calculation parameters — Calculation method FE-C.

Test series			$F_{u,exp,b}$	Calculation parameters[a]								$F_{u,cal,b}$
			[kN]	f_t^I [N/mm²]	f_t^{II} [N/mm²]	$G_{c,t}^I$ [N/mm]	$G_{c,t}^{II}$ [N/mm]	f_c^I [N/mm²]	f_c^{II} [N/mm²]	$G_{c,c}^I$ [N/mm]	$G_{c,c}^{II}$ [N/mm]	[kN]
V1	-01		95.0	*1.89*	1.25·5.24	*0.30*	*0.23*·f_t^{II}	2.59	2.0·f_c^I	*0.15*	*0.29*·f_c^I	80.1
	-02		86.8	*1.89*	1.25·5.24	*0.30*	*0.23*·f_t^{II}	2.59	2.0·f_c^I	*0.15*	*0.29*·f_c^I	80.1
	-03		91.2	*1.89*	1.25·5.24	*0.30*	*0.23*·f_t^{II}	2.60	2.0·f_c^I	*0.15*	*0.29*·f_c^I	80.2
	-04		93.5	*1.89*	1.25·5.24	*0.30*	*0.23*·f_t^{II}	2.98	2.0·f_c^I	*0.15*	*0.29*·f_c^I	80.6
	-05		91.4	*1.89*	1.25·5.24	*0.30*	*0.23*·f_t^{II}	3.03	2.0·f_c^I	*0.15*	*0.29*·f_c^I	80.7
	-06		93.3	*1.89*	1.25·5.24	*0.30*	*0.23*·f_t^{II}	4.16	2.0·f_c^I	*0.15*	*0.29*·f_c^I	80.8
V2			109.3	*1.89*	1.25·*6.10*	*0.30*	*0.23*·f_t^{II}	–	–	–	–	94.8
V3	-01		106.9	*1.89*	1.25·6.50	*0.30*	*0.23*·f_t^{II}	3.25	2.0·f_c^I	*0.15*	*0.29*·f_c^I	98.8
	-02		124.5	*1.89*	1.25·6.50	*0.30*	*0.23*·f_t^{II}	3.64	2.0·f_c^I	*0.15*	*0.29*·f_c^I	99.9
V4	-01	2EP	54.4	*1.89*	1.25·*6.10*	*0.30*	*0.23*·f_t^{II}	3.25	2.0·f_c^I	*0.15*	*0.29*·f_c^I	45.7
		PM	61.8	*1.89*	1.25·*6.10*	*0.30*	*0.23*·f_t^{II}	3.25	2.0·f_c^I	*0.15*	*0.29*·f_c^I	45.1
		PRF	45.8	*1.89*	1.25·*6.10*	*0.30*	*0.23*·f_t^{II}	3.25	2.0·f_c^I	*0.15*	*0.29*·f_c^I	45.9
	-02	2EP	60.0	*1.89*	1.25·*6.10*	*0.30*	*0.23*·f_t^{II}	4.07	2.0·f_c^I	*0.15*	*0.29*·f_c^I	45.7
		PM	50.7	*1.89*	1.25·*6.10*	*0.30*	*0.23*·f_t^{II}	4.07	2.0·f_c^I	*0.15*	*0.29*·f_c^I	45.2
		PRF	48.3	*1.89*	1.25·*6.10*	*0.30*	*0.23*·f_t^{II}	4.07	2.0·f_c^I	*0.15*	*0.29*·f_c^I	46.0
	-03	2EP	47.9	*1.89*	1.25·*6.10*	*0.30*	*0.23*·f_t^{II}	4.20	2.0·f_c^I	*0.15*	*0.29*·f_c^I	45.7
		PM	53.3	*1.89*	1.25·*6.10*	*0.30*	*0.23*·f_t^{II}	4.20	2.0·f_c^I	*0.15*	*0.29*·f_c^I	45.2
		PRF	53.4	*1.89*	1.25·*6.10*	*0.30*	*0.23*·f_t^{II}	4.20	2.0·f_c^I	*0.15*	*0.29*·f_c^I	46.0
	-04	2EP	47.0	*1.89*	1.25·*6.10*	*0.30*	*0.23*·f_t^{II}	3.16	2.0·f_c^I	*0.15*	*0.29*·f_c^I	45.7
		PM	49.1	*1.89*	1.25·*6.10*	*0.30*	*0.23*·f_t^{II}	3.16	2.0·f_c^I	*0.15*	*0.29*·f_c^I	44.9
		PRF	50.5	*1.89*	1.25·*6.10*	*0.30*	*0.23*·f_t^{II}	3.16	2.0·f_c^I	*0.15*	*0.29*·f_c^I	45.9
V5	-01		109.5	*1.89*	1.25·4.40	*0.30*	*0.23*·f_t^{II}	1.99	2.0·f_c^I	*0.15*	*0.29*·f_c^I	105.8
	-02		63.6	*1.89*	1.25·4.40	*0.30*	*0.23*·f_t^{II}	1.99	2.0·f_c^I	*0.15*	*0.29*·f_c^I	52.9
V6	-01		87.3	*1.89*	1.25·4.93	*0.30*	*0.23*·f_t^{II}	3.05	2.0·f_c^I	*0.15*	*0.29*·f_c^I	64.4
	-02		80.2	*1.89*	1.25·4.93	*0.30*	*0.23*·f_t^{II}	3.05	2.0·f_c^I	*0.15*	*0.29*·f_c^I	64.4
	-03		91.3	*1.89*	1.25·4.93	*0.30*	*0.23*·f_t^{II}	–	–	–	–	76.1
V7	-01		102.8	*5.50*	1.36·*11.00*	*1.39*	*0.23*·f_t^{II}	3.05	2.0·f_c^I	*0.15*	*0.29*·f_c^I	79.9
	-02		112.2	*5.50*	1.36·*11.00*	*1.39*	*0.23*·f_t^{II}	3.05	2.0·f_c^I	*0.15*	*0.29*·f_c^I	79.9

[a] Italicized values were assumed based on data from relevant literature sources.

CRediT authorship contribution statement

Jens Frohnmüller: Writing – original draft, visualization, validation, software, methodology, investigation, formal analysis, data curation, conceptualization. **Werner Seim:** Writing – review & editing, supervision, methodology, funding acquisition, conceptualization.

Declaration of competing interest

The authors declare the following financial interests/personal relationships which may be considered as potential competing interests: Werner Seim and Jens Frohnmüller report, that financial support was provided by the University of Kassel.

Data availability

Data will be made available on request.

References

[1] J. Frohnmüller, W. Seim, J. Gaida, A. Ho, L. Völlmecke, Entwicklung einer Schnellbaumethode für HBV-Decken mittels Verklebung vorgefertigter Betonbauteile, Research report, University of Kassel, University of Kassel in cooperation with Bewo - Betonwerk Oberessendorf GmbH & Co. KG, 2022.

[2] J. Frohnmüller, W. Seim, Pilot tests on the suitability of a commercially available epoxy resin for adhesively bonded timber-concrete composites, Technical report, University of Kassel, fischerwerke GmbH & Co. KG, 2022.

[3] J. Frohnmüller, W. Seim, C. Umbach, J. Hummel, Adhesively bonded timber-concrete composite construction method (ATCC) - pilot application in a school building in Germany, in: Proc., 17th World Conf. on Timber Eng.: WCTE 2023, Oslo, Norway, 2023, http://dx.doi.org/10.52202/069179-0542.

[4] M. Schäfers, Entwicklung von hybriden Bauteilen aus Holz und hochfesten bzw. ultrahochfesten Betonen (Ph.D. thesis), University of Kassel, 2010, http://dx.doi.org/10.17170/kobra-202012182711.

[5] M. Kästner, Zum Tragverhalten von Polymermörtel - Klebverbindungen für die Anwendung bei Straßenbrücken in Holz-Beton-Verbundbauweise (Ph.D. thesis), Bauhaus University of Weimar, 2019.

[6] Q. Fu, L. Yan, B. Kasal, Testing methods for shear strength of bond line between concrete and different types of engineered wood, Int. J. Adhes. 102 (102671) (2020) http://dx.doi.org/10.1016/j.ijadhadh.2020.102671.

[7] J. Frohnmüller, J. Fischer, W. Seim, Full-scale testing of adhesively bonded timber-concrete composite beams, Mater. Struct. 54 (187) (2021) http://dx.doi.org/10.1617/s11527-021-01766-y.

[8] J. Frohnmüller, G. Wisner, T. Waschkowitz, M. Mérono, E. Stammen, K. Dilger, Durability of adhesively bonded timber-concrete-composite constructions joined by fast heated structural adhesive bond lines, ASTM - Selected Technical Papers STP 1633 (2022) 128–151, http://dx.doi.org/10.1520/STP163320200063.

[9] L. Eisenhut, W. Seim, S. Kühlborn, Adhesive-bonded timber-concrete composites - Experimental and numerical investigation of hygrothermal effects, Eng. Struct. 125 (2016) 167–178, http://dx.doi.org/10.1016/j.engstruct.2016.05.056.

[10] T. Tannert, A. Gerber, T. Vallée, Hybrid adhesively bonded timber-concrete-composite floors, Int. J. Adhes. 97 (102490) (2020) http://dx.doi.org/10.1016/j.ijadhadh.2019.102490.

[11] L. Eisenhut, Geklebter Verbund aus Holz und hochfestem Beton - Untersuchungen zum Langzeitverhalten (Ph.D. thesis), University of Kassel, 2015, http://dx.doi.org/10.19211/KUP9783862199952.

[12] G. Wisner, E. Stammen, K. Dilger, J. Frohnmüller, W. Seim, M. Mérono, C. Link, Wirtschaftliche Herstellung hochwertiger Holz-Beton-Verbundelemente unter Anwendung einer innovativen Schnellklebtechnik und Einsatz von Laubholz - SpeedTeCC (IGF Nr. 19417N), Research report, Int. Verein für Techn. Holzfragen e.V., 2021.

[13] P. Grönquist, Tragverhalten von verklebten Holz-Beton- und Holz-Polymerbeton Verbunddecken mit Buchen-Stabschichtholz, in: S-WIN, Swiss Wood Innovation Network, Zürich, Schweiz, 2022, http://dx.doi.org/10.3929/ethz-b-000616135.

[14] J. Frohnmüller, W. Seim, M. Mérono, G. Wisner, E. Stammen, Adhesively bonded timber-concrete composites with smooth concrete surfaces, in: Proc., 16th World Conf. on Timber Eng.: WCTE 2021, Santiago de Chile, Chile, 2021.

[15] J.H. Negrão, F.M. Oliveira, C.A. Oliveira, P.B. Cachim, Glued composite timber-concrete beams. I: Interlayer connection specimen tests, J. Struct. Eng. 136 (2010) 1236–1245, http://dx.doi.org/10.1061/(ASCE)ST.1943-541X.0000228.

[16] R. Shrestha, J. Mak, K. Crews, Experimental investigations on epoxy bonded shear connection for TCCs, in: Proc., 12th World Conf. on Timber Eng.: WCTE 2012, Auckland, Neuseeland, 2012.

[17] K. Śliwa-Wieczorek, W. Derkowski, E. Binder, A. Kwiecien, B. Zajac, E. Halilovic, S. Lotinac, Shear stiffness and capacity of PU flexible joint in TCCs, in: Building for the Future: Durable, Sustainable, Resilient, Springer Nature Switzerland, Cham, 2023, pp. 476–485, http://dx.doi.org/10.1007/978-3-031-32519-9_46.

[18] F. Brosch, B. Kromoser, Usability and suitability of different small-scale test setups to accurately assess the shear strength of the glue line in adhesive bonded timber-concrete-composite elements, in: Building for the Future: Durable, Sustainable, Resilient, Springer Nature Switzerland, Cham, 2023, pp. 219–226, http://dx.doi.org/10.1007/978-3-031-32519-9_20.

[19] EN 1992-1-1, Eurocode 2: Design of concrete structures - Part 1-1: General rules and rules for buildings; German version EN 1992-1-1:2004 + AC:2010, 2011.

[20] TS 19103, Eurocode 5: Design of Timber structures - structural design of timber-concrete composite structures - Common rules and rules for buildings, 2021, CEN TS 19103, CEN Technical Committee 250.

[21] C. Hackspiel, Verklebung als Verbund für Holz-Beton-Deckensysteme, in: 1. Holzbau Kongress Berlin DHK 2020, Berlin, 2020.

[22] D. Zauft, Untersuchungen an geklebten Verbundkonstruktionen aus Holz und Leichtbeton (Ph.D. thesis), Shaker Verlag Aachen, University of Berlin, 2014.

[23] H.-J. Blaß, O. Krüger, Schubverstärkungen von Holz mit Holzschrauben und Gewindestangen, in: Karlsruher Berichte zum Ingenieurholzbau, Vol. 15, University of Karlsruhe, 2010, http://dx.doi.org/10.5445/KSP/1000020518.

[24] R. Spengler, Festigkeitsverhalten von Brettschichtholz unter zweiachsiger Beanspruchung Teil 1 - Ermittlung des Festigkeitsverhaltens von Brettelementen aus Fichte durch Versuche, in: Berichte zur Zuverlässigkeitstheorie der Bauwerke, University of Munich, 1982.

[25] S. Akter, T. Bader, Experimental assessment of failure criteria for the interaction of normal stress perp. to the grain with rolling shear stress in Norway spruce, Eur. J. Wood Wood Prod. 78 (2020) 1105–1123, http://dx.doi.org/10.1007/s00107-020-01587-w.

[26] SIA 265, Holzbau, Schweizerischer Ingenieur- und Architektenverein (SIA), Schweizerische Normen-Vereinigung (SNV), 2012, SIA 265, Zurich.

[27] S. Austin, P. Robins, Y. Pan, Shear bond testing of concrete repairs, Cem. Concr. Res. 29 (7) (1999) 1067–1076, http://dx.doi.org/10.1016/S0008-8846(99)00088-5.

[28] EN 408, Timber structures - Structural timber and glued laminated timber - Determination of some physical and mechanical properties; German version EN 408:2010+A1:2012, 2012, EN 408.

[29] DIN 1542, Products and systems for the protection and repair of concrete structures - Test methods - Measurement of bond strength by pull-off; German version EN 1542: 1999, 1999.

[30] DIN 1048-2, Testing methods for concrete; hardened concrete in structures and components, 1991, DIN 1048-2, (2015-09 withdrawn without replacement).

[31] G. Valentin, L. Boström, P. Gustafsson, A. Ranta-Maunus, S. Gowda, Application of Fracture Mechanics to Timber Structures. Rilem State-Of-The-Art Report, TC 110-TFM, Techn. Research Centre of Finland, 1991.

[32] T. Claus, Entwurf und Berechnung von ausgeklinkten Trägerauflagern und Zapfenverbindungen im Holzbau (Ph.D. thesis), University of Kassel, 2020, http://dx.doi.org/10.17170/kobra-202009281850.

[33] EN 12390-3, Testing hardened concrete - Part 3: Compressive strength of test specimens; German version EN 12390-3:2019, 2019.

[34] R. Jockwer, R. Steiger, A. Frangi, J. Köhler, Impact of material properties on the fracture mechanics design approach for notched beams in EC 5, in: Proc. of CIB-W18/44, Vol. 44-6-1, Alghero, Italy, 2011.

[35] H.-J. Blaß, M. Schmid, Querzugfestigkeit von Vollholz und Brettschichtholz, Holz a. Roh- u. Werkst. 58 (6) (2001) 456–466, http://dx.doi.org/10.1007/s001070050460.

[36] M. Westermayr, F. Hunger, J. Van de Kuilen, Strength and stiffness perp. to the grain of ash (Fraxinus e.) and beech (Fagus s.) in comparison to spruce (Picea a.), in: 6th Int. Scientific Conf. on Hardwood Processing, Lahti, Finland, 2017.

[37] P. Glos, J. Denzler, Kalibrierung der charakteristischen Schubfestigkeitskennwerte für Vollholz in EN 338 entsprechend den Rahmenbedingungen der nationalen Sortiernorm, Research report, Institute for wood research, Munich, 2004.

[38] G. Mirzaei, B. Mohebby, M. Tasooji, The effect of hydrothermal treatment on bond shear strength of beech wood, Eur. J. Wood Wood Prod. 70 (2012) 705–709, http://dx.doi.org/10.1007/s00107-012-0608-9.

[39] DIN 68364:2003-05, Properties of wood species - Density, modulus of elasticity and strength, German version, 2003, DIN 68364.

[40] H.J. Windeck, Querdruckverhalten von Brettschichtholz aus Nadelholz, Bautechnik 94 (11) (2017) 767–775, http://dx.doi.org/10.1002/bate.201700048.

[41] U. Hübner, Mechanische Kenngrößen von Buchen-, Eschen- und Robinienholz für lastabtragende Bauteile (Ph.D. thesis), University of Graz, 2014.

[42] S. Ammann, P. Niemz, Specific fracture energy at glue joints in European beech wood, Int. J. Adhes. 60 (2015) 47–53, http://dx.doi.org/10.1016/j.ijadhadh.2015.03.007.

[43] MC-10, Model Code for Concrete Structures 2010, Fédération Internationale Du Béton: Fib, 2013, MC-10, Fédération internationale du Béton: fib.

[44] K. Zilch, R. Niedermeier, Formulierung von Prüfgrundsätzen bei Verbundversuchen mit oberflächig aufgeklebten Stahllaschen und CFK-Lamellen, Research report, Fraunhofer-IRB-Verlag, Stuttgart, 2006.

[45] G. Habenicht, Kleben - Grundlagen, Technologien, Anwendungen, Springer-Vieweg Verlag, Berlin, Heidelberg, 2009.

[46] EN 26891, Timber structures; joints made with mechanical fasteners; general principles for the determination of strength and deformation characteristics (ISO 6891:1983); german version EN 26891:1991, 1991.

[47] J. Frohnmüller, W. Seim, Innovative prefabricated timber-concrete composite elements with adhesive bond, in: Proceedings 66th BetonTage, BFT International, Vol. 2022, 2022, p. 103.
[48] M. Braun, Optimierung der Fugengeometrie von geklebten Holz-Beton-Verbundbauteilen mit Verbund durch Fugenverguss, Master thesis, University of Kassel, 2020.
[49] M. Mérono, C. Link, G. Wisner, E. Stammen, K. Dilger, J. Frohnmüller, W. Seim, Innovative Heißklebung von tragenden Holz-Beton-Verbundelementen, Adhäsion Kleben & Dichten 63 (2019) 30–34, http://dx.doi.org/10.1007/s35145-019-0083-0.
[50] D. Glasner, A. Ringhofer, R. Brandner, G. Schickhofer, Contribution to the testing, evaluation and design of cross laminated timber (CLT) in respect to rolling shear, in: Proc., 55th INTER Conference, Bad Aibling, Germany, 2022.
[51] P. Glos, J. Denzler, Characteristic shear strength values based on tests according to EN1193, in: Proc. of CIB-W18/36, Vol. 36-6-1, Colorado, USA, 2003.
[52] G. Schickhofer, Determination of shear strength values for GLT using visual and machine graded spruce laminations, in: Proc. of CIB-W18/34, Vol. 34-12-6, Venice, Italy, 2001.
[53] S. Rahman, M. Ashraf, M. Subhani, Comparison between actual and equivalent crack resistance R-curves for timber and timber bond under mode-II fracture, in: Proc., 17th World Conf. on Timber Eng.: WCTE 2023, Oslo, Norway, 2023, http://dx.doi.org/10.52202/069179-0021.